Numerical Study of $BaZrS_3$ Based Chalcogenide Perovskite Solar Cell Using SCAPS-1D Device Simulation

Najwa Chawki (chawki.najwa@gmail.com)
Mohammed V University https://orcid.org/0000-0003-3005-1346
Mustapha Rouchdi
Mohammed V University
Boubker Fares
Mohammed V University

Research Article

Keywords: BaZrS3, Hole transport material (HTM), Electron transport material (ETM), SCAPS-1D, Power conversion efficiency, Fill factor

Posted Date: January 18th, 2022

DOI: https://doi.org/10.21203/rs.3.rs-1251663/v1

Abstract

Chalcogenide perovskites are prototypical absorber materials based solar cells, they could solve both: the stability and toxicity issues existing in conventional perovskites. A device simulation of $BaZrS_3$ as a potential absorbing material (high chemical stability, direct band gap and a strong light absorption coefficient) based chalcogenide perovskite solar cells is performed by using the one dimensional Solar Cell Capacitance Simulator (SCAPS)-1D software. Parameters like (thickness, doping concentration, defect density of the absorber and interfaces, temperature) are varied in order to inspect their impact on device performance. For this study, a performed architecture has been proposed: FTO (Fluorine doped Tin Oxide)/TiO_2 (ETL; Electron Transport Layer)/$BaZrS_3$ (Absorber)/Spiro-OMeTAD (HTL; Hole Transport Layer)/Au (metal back contact). To enhance the solar cell efficiency, an optimization of these key parameters is investigated. Our simulation results in optimized thickness and doping density (N_A, N_D) of (80 nm; 1×10^{19} cm^{-3}), (10 nm; 8×10^{19} cm^{-3}), (850 nm; 1×10^{20} cm^{-3}) and (60 nm; 9×10^{19} cm^{-3}) for FTO, TiO_2, $BaZrS_3$ and Spiro-OMeTAD materials respectively, with a global illumination spectrum AM1.5 and 440 K as an optimum operation temperature, are found to be: PCE (maximum Power Conversion Efficiency) of 17.29%, FF (fill factor) of 86.26%, *Voc* (Open Circuit Voltage) of 1.2124 V and *Jsc* (Short Circuit current density) of 16.5363 mA/cm^2.

1. Introduction

Boosting the efficiency and minimizing the energy lost in solar cells devices are the most issues in the research community of chemistry and physics, in order to enhance the performance of energy harvesting and sensing materials. Perovskite solar cell has emerged as a third generation thin film photovoltaic solar cells, in the aim of discovering new and better performing materials, to solve the high fabrication cost, low efficiency and toxicity presented in the conventional ones: such as mono and poly crystalline silicon constituted the first generation, thin film solar cells based on CdTe, CIGS or amorphous silicon as the second generation. Perovskite could be an absorbent material for solar cells, fabricated as both single and multi (tandem) junction. It is generally represented by the chemical formula ABX_3 (A and B: cations with different size, X: anion bonded to both). The hybrid (organic- inorganic) lead halide perovskites are considered as a major scientific breakthrough in the development of absorber photovoltaic materials owing to their interesting optoelectronic properties. However, a PCE increased from 3.8% in 2009 [1] to above 26.7% in 2019 [2], they suffer from intrinsic instability due to the use of organic cations like methyl-ammonium, which degraded face to humidity or oxygen or heat exposure, and the toxicity of lead (Pb). The proposed approach to solve these issues was finding a new type of perovskite materials (inorganic) with an appropriate Goldschmidt tolerance criteria, abundant and nontoxic devices, with an efficiency similar to lead-based perovskites. Among them, chalcogenide perovskites ABX_3 (A= Ca, Sr, or Ba; B= Ti, Zr, or Hf; X =S or Se). They combine both: the good optoelectronic properties of halide and the good stability of oxides, owing to an appropriate optical band gap, high absorption coefficient and facile charge transport. Some of them were the subject of experimental investigations such as $BaZrS_3$, $SrZrS_3$, $CaZrS_3$,

$SrTiS_3$ and $CaSnS_3$ [3]. Recently, $BaZrS_3$ is the most studied chalcogenide compound for optoelectronic applications.

Kuhar et al. [4] screened eight direct band gap chalcogenide perovskites, into consideration based on stability (formation energy), light absorption (band gap), charge mobility (effective masses) and defect tolerance (defects states in the gap). Among them, $BaZrS_3$ in the $GdFeO_3$ structure [4]. A similar screening work was done by Buffiere et al.[5]. On the other hand, Swanrkar et al. [6] synthesized and characterized successfully Zr-chalcogenides like $BaZrS_3$ and $SrZrS_3$, as a result they found that the calculated band gap is reduced from 3.9 eV for $BaZrO_3$ to around 1.7 eV for $BaZrS_3$ after sulfurization, with a strong light absorption. The calculated PCE of $BaZrS_3$ as a function of the absorber thickness (from 0 to 3 μm) is around 26% with a band gap equal to 1.85 eV. However, this PCE is smaller than that corresponding to $MAPbI_3$ (∼29%)[6]. The efficiency of our chalcogenide could be improved by reducing the band gap whereas alloying by substituting S with Se or Zr with Ti. For instance, Wei et al. [7] incorporated and described Ti-alloyed $Ba(Zr_{(1-x)}Ti_{(x)})S_3$, with a range of x from (0 to 0.1), a theoretical PCE of 32% was achieved, thanks to a reduction of band gap from 1.78 to 1.51 eV (reached the Shockley–Queisser limit of a single-junction solar cell). The same work was done by Zitouni et al. [8] using the DFT (Density Functional Theory), they investigated the optoelectronic properties of $BaZrS_{(3-x)}Se_{(x)}$ doped with Se (x = 0%, 10%, 15% and 20%). As a result, they obtained that the band gap decreases successfully by increasing the percentage of doping from 1.59 eV for 0% of Se to 1.37 eV for 20% of Se. Moreover, they concluded that $BaZrS_3$ doped with Se (p-type material) is a good absorber for PV applications [8].

The aim of our work is to study the simulation of $BaZrS_3$ based chalcogenide perovskite as an absorber for solar cell, by using SCAPS-1D (version 3.3.08) software, to address commercialization challenges by optimizing parameters (thickness, doping density, defect density, temperature) for all: the absorber, FTO, HTM and ETM.

2. Computational Details

The Solar cell capacitance simulator SCAPS-1D is a one dimensional solar cell simulation program, developed at the department of Electronics and Information Systems (ELIS); University of Gent, Belgium. This software is based on three coupled differential equations: Poisson’s (1), continuity equations for holes (2) and electrons (3).

$$\frac{d}{dx}\left(\varepsilon(x)\frac{d\Psi}{dx}\right) = q[p(x) - n(x) + ND^{+}(x) - NA^{-}(x) + pt(x) - nt(x)] \quad (1)$$

$$\frac{1}{j}\frac{dJp}{dx} + Rp(x) - G(x) \quad (2)$$

$$-\frac{1}{j}\frac{dJn}{dx} + Rn(x) - G(x) \quad (3)$$

With: ε is the permittivity, q: the charge of electrons, Ψ: the electrostatic potential, n and p: the free electrons and holes, n_t and p_t: the trapped electrons and holes, N_D^+ and N_A^- the ionized donor and acceptor as doping concentrations, R_n and R_p: the electron and hole recombination rates, G: the generation rate, J_n and J_p: the electron and hole current densities.

3. Simulation Parameters

We have chosen as an architecture of the solar cell: FTO/TiO_2 (ETM)/$BaZrS_3$ (chalcogenide perovskite material)/Spiro-OMeTAD (HTM)/Au (metal back contact), as shown in **Fig. 1**. Parameters for such devices (FTO, ETM, $BaZrS_3$, HTM) such as: thickness, band gap, electron affinity, dielectric permittivity, CB and VB effective densities of states, electron and hole motilities, shallow acceptor and donor densities (doping concentration) N_A and N_D respectively, and defect density N_t are listed in Table 1, in order to have a successful simulation result, these values need to be chosen very attentively. In this work, we are used these key parameters mostly from fabrication based works published in referred journals. Other parameters such as electron and hole thermal velocities are assumed to be the same for all layers (=10^7cm/s). Moreover, we introduced the Spiro-OMeTAD/$BaZrS_3$ and $BaZrS_3$/TiO_2 interfaces defect layers (IDLs), as illustrated in Table 2, to simplify the simulation process we considered neutral defect at the interfaces.

Each layer in this structure is essential for the proper functioning of the photovoltaic cell (PV). Fluorine doped tin oxide FTO is used as an anode (front contact), a type of inorganic transparent conducting oxides thin film of optically transparent and electrically conductive material. It has a wide band gap, n-type conductivity. and a work function assumed to be 4.4 eV [9]. To separate electron-hole pairs created in perovskite we used an ETL which injects photo generated electron into n-type semiconductor such as ZnO [10], SnO_2 [11] and TiO_2 [12], in order to block holes and prevent them from reaching the FTO, as this would short- circuit the cell. Generally, TiO_2 is commonly the most used as ETL because of its high transparency, excellent carrier separation ability, environmental stability, and easy fabrication process [12]. It is composed of effective electron injection because of its appropriate conduction band and high electron mobility [12]. Therefore, TiO_2 is generally used between the FTO conducting substrate and perovskite layer. We used the inorganic chalcogenide perovskite $BaZrS_3$ as the absorber material for our structure, in order to demonstrate its suitable optoelectronic properties as a promising material for photovoltaic solar cells. Electron-hole pairs are created in the absorber following light absorption can

possibly result in the formation of excitons. The role of HTL is the injection of holes into a p-type semiconductor material such as Spiro-OMeTAD, an electron blocking layer to separate charge created in the perovskite. It is the most used HTM in photovoltaic solar cells because of its low cost, ease of fabrication and high performance [13]. The gold (Au) is used as a cathode (back contact) with a work function assumed to be 5.1eV.

We have selected for all simulation, AM 1.5G spectrum with an incident power of 1000 W/m^2 and an operation temperature of 300 K, with no consideration of radiative band to band recombination and Auger recombination, only the defect mechanism was considered.

Table 1
Basic parameters used in the SCAPS-1D simulation for each layer

Parameters	FTO[9]	TiO_2[2]	$BaZrS_3$[14]	Spiro-OMeTAD [15]
Thickness (nm)	Wide-range	Wide-range	Wide-range	Wide-range
Band gap (eV)	3.5	3.2	1.7	3.04
Electron affinity (eV)	4	4	4.5	2.11
Dielectric Permittivity (relative)	9	100	4.19	3
CB effective density of states (cm^{-3})	2.2×10^{18}	1×10^{21}	2.2×10^{18}	2.2×10^{18}
VB effective density of states (cm^{-3})	1.8×10^{19}	2×10^{20}	1.8×10^{19}	1.8×10^{19}
Electron mobility (cm^2/Vs)	20	6×10^{-3}	11.3	1×10^{-3}
Hole mobility (cm^2/Vs)	10	6×10^{-3}	5.58	1×10^{-3}
Shallow uniform donor density $N_D(cm^{-3})$	Wide-range	Wide-range	0	0
Shallow uniform acceptor density $N_A(cm^{-3})$	0	0	Wide-range	Wide-range
Defect density Nt (cm^{-3})	1×10^5	1×10^5	Wide-range	1×10^5

Table 2
Defect density at the interface

Interface	Spiro-OMeTAD/$BaZrS_3$	$BaZrS_3/TiO_2$
Defect type	Neutral	Neutral
Capture cross section for electron and holes (cm^{-2})	10^{-5}	10^{-5}
Energetic distribution	Single	Single
Reference for defect energy level Et	above the highest EV	above the highest EV
Total density (cm^{-3})	Wide-range	Wide-range

$BaZrS_3$ crystallizes in an orthorhombic structure with lattice parameters of a=7.088Å, b=7.155Å and c=10.044Å under *Pnma* space group [16] (Fig. 2), traced by Vesta (software configuration management). The band structure and the density of states shown in Fig. 3 indicate a direct band gap of ~1.7 eV. The maximum absorption value for $BaZrS_3$ is found to be 5.9×10^5 cm^{-1} obtained at ultraviolet light (λ = 276 nm)[8].

4. Results And Discussion

4.1. Effect of changing the thickness of each layer on the PCE and FF

The thickness of the absorber is one of the most important parameters in the simulation, it has an interesting influence on the performance of the solar cell. Here, we focus on the PCE and the FF, as the most important parameters in the PV solar cell, they can be obtained by the equations (4) and (5) bellow [17]:

$$PCE = \frac{P_{out}}{P_{in}} = \frac{V_{OC} \times J_{SC} \times FF}{P_{in}} \quad (4)$$

$$FF = \frac{V_{MP} \times J_{MP}}{V_{OC} \times J_{SC}} \quad (5)$$

With, V_{MP} and J_{MP} are the voltage and the current density at the maximum power.

In order to observe this effect, we varied the thickness of (absorber, HTL, ETL and FTO) keeping other parameters constant, as illustrated in Fig. 4. **(a), (b), (c), and (d)**. The device performance is optimized in this section as a function of thickness. It is worthy to mention, that for each simulation we used the optimized value found by the previous one.

Figure 4. **(a)**, shows the effect of the absorber thickness on the PCE and FF varied from 100 nm to 4500 nm, it can be noticed that with absorber thickness increasing, the PCE increases continuously, it isn't the same case for the FF which varies in a random way. Our results indicate an optimized thickness of 850

nm which gives both: a maximum PCE (15.83%) and FF (88.7%). For the purpose of absorbing a maximum number of photons and generating an important amount of electron-hole pair, the absorber thickness must be increased. The reduced thickness leads to a very close depletion layer which increases the recombination rate consequently the PCE decrease [18]. However, the variation of the FF with the absorber thickness is due to the series resistance [18]. As the series resistance increases FF decreases [18].

It is worth mentioning that the FF varies in a random way for all (HTL, ETL and FTO) in Fig. 4. **(b), (c) and (d).**

It can be deduced from the effect of HTL thickness varying from 10 nm to 500 nm, **(**Fig. 4. **(b))** that the PCE increases with increasing of the thickness up to 30 nm, then it decreases after this value. Actually, Spiro-OMeTAD (organic HTM) acquires low conductivity and low charge carrier mobility as compared to the inorganic HTMs [2]. Consequently, the increased thickness will increase the resistance of the layer. Thus, it will decrease the PCE [2]. As an optimized thickness we have selected 60 nm corresponding to a PCE of 15.8328% and a FF of 88.697%.

The thickness in the case of ETL was studied from 3 nm to 100 nm, as illustrated in Fig. 4. **(c).** It can be observed that the PCE decreases by increasing this later. The lower transmittance in 300–400 nm range of TiO_2 and its low electron mobility, leads to the absorption of incident light by thicker ETL [2]. Therefore, reduction in PCE value was remarked as a function of increase in TiO_2 thickness [2]. We continued our simulation with a small thickness of TiO_2 (10 nm) which gives a PCE of 15.8336% and a FF of 87.133%.

Figure 4. **(d)**, indicate the effect of FTO thickness varied from 10 nm to 500 nm. A reduction of the PCE with increasing of the thickness was also realized. Similar to ITO [19], if its thickness increases, its sheet resistance will decrease while its optical transmittance decreases [19]. Consequently, the PCE also decreases. As an optimum value of FTO thickness we have selected 80 nm that delivers a PCE of 15.8151% and a FF of 88.697%.

To finish this section, we can mention that the influence of thickness on the performance is more important for the absorber (the active layer) than for the other layers (FTO, ETL, and HTL). This confirms that the absorber is the key component in the PSC which is coherent with other researches [18], [20], [21], [22].

4.2. Effect of doping densities on the PCE and FF

The plot of PCE and FF parameters as a function of dopant concentrations N_A and N_D for each layer (absorber, HTM, ETM and FTO) is shown in Fig. 5. **(a), (b), (c) and (d)**, respectively. The study has been carried out from 1×10^{19} cm^{-3} to 3×10^{20} cm^{-3} due to a very low performance below 10^{19} cm^{-3}. The strategy chosen to improve the efficiency is doping, which boost the electronic properties. Doping in the solar cell affect its performance. It enhances the electrical behavior of the layers because it increases the conductivity of majority carriers which improve the PCE [23]. As illustrated in Fig. 5, the PCE for all

($BaZrS_3$, Spiro-OMeTAD, TiO_2 and FTO) increases with doping densities. However, this variation still negligible for (HTM, ETM and FTO) compared to the absorber $BaZrS_3$, as we can see in Fig. 6, because the absorber is the key component in the PVS and its higher doping density decrease the band gap which increase the PCE [7] [21]. Our optimized doping concentrations are: 1×10^{20} cm^{-3} for the absorber, 9×10^{19} cm^{-3} for HTM, 8×10^{19} cm^{-3} for ETM and 1×10^{19} cm^{-3} for FTO. These values are chosen as it is difficult to obtain higher doping practically.

4.3. Effect of defect density of the absorber and interfaces on the PCE

Our simulation results indicated that the defect density Nt (a limiting factor to achieving the Shockley-Queisser limit) influences the performance of PV solar cell, this defect density affect directly the absorber (the active layer) layer and it is invariable for the other layers (ETL, HTL, FTO). An optimized value of this parameter is required to enhance the performance of the architecture. The Table 3, confirmed that the PCE decreases from 15.81–8.17% with increasing the defect density of $BaZrS_3$ from 10^{13} cm^{-3} to 10^{17} cm^{-3}. When defect density decreases, carrier life time will increases. Therefore, less recombination and higher PCE are obtained [24]. The PCE still constant for (Nt =10^{10} cm^{-3}, 10^{11} cm^{-3}, 10^{12} cm^{-3} and 10^{13} cm^{-3}), thus we selected 10^{13} cm^{-3} as the optimized value for the defect density of $BaZrS_3$ which distribute a PCE of 15.81%.

The quality of interface layers has a crucial impact on the performance of the solar cell. The defects on these interfaces deteriorate its quality then increase the rate of recombination. In order to manifest the validity of the simulation, all influencing parameters must be optimized. In this section, we studied the effect of two interfaces defect densities on the PCE (from 10^{10} cm^{-2} to 10^{17} cm^{-2}): that of HTM/$BaZrS_3$ illustrated in Table 4. **(a)**, and that of $BaZrS_3$/ETL in Table 4. **(b).** It can be deduced that the defect density of the Spiro-OMeTAD/$BaZrS_3$ interface has a mild impact on the PCE below 10^{16} cm^{-2} thus we have chosen 10^{15} cm^{-2} as the optimum value. In contrast, the defect density of $BaZrS_3$/TiO_2 interface has a remarkable influence on the PCE. The number of electron-hole pairs generated at $BaZrS_3$/TiO_2 is more important than that of HTL/$BaZrS_3$ which increases the recombination rate [20], automatically the PCE will be reduced. In the aim of optimizing our simulation parameters we have selected a lower interface defect density of 10^{11} cm^{-2} with a higher PCE of 15.81% for $BaZrS_3$/ETL.

Table 3
Variation in PCE according to variation in defect density of $BaZrS_3$

Nt (cm^{-3})	10^{10}	10^{11}	10^{12}	10^{13}	10^{14}	10^{15}	10^{16}	10^{17}
PCE (%)	15.81	15.81	15.81	15.81	15.78	15.49	13.52	8.17

Table 4
(a) Effect of HTL/$BaZrS_3$ interface defect density on the PCE

Spiro-OMeTAD/$BaZrS_3$ (cm^{-2})	10^{10}	10^{11}	10^{12}	10^{13}	10^{14}	10^{15}	10^{16}	10^{17}
PCE (%)	15.81	15.81	15.81	15.81	15.81	15.81	15.806	14.85

Table 4
(b) Effect of $BaZrS_3$/ETL interface defect density on the PCE

$BaZrS_3/TiO_2$ (cm^{-2})	10^{10}	10^{11}	10^{12}	10^{13}	10^{14}	10^{15}	10^{16}	10^{17}
PCE (%)	15.81	15.81	15.80	15.71	15.25	14.44	13.82	13.65

4.4. Effect of temperature on the PCE and FF of the cell

We have also reported the effect of temperature on the performance of our simulation. Working temperature has an important effect on the solar cell, then on the thermal stability in the device. Generally, 300 K is taken as a standard value for temperature, but the solar cell during its operation can be subjected to high temperatures. Therefore, we have varied temperature from 300 K to 500 K, in order to observe its impact on the PCE and FF, as shown in Fig. 7. We noticed that the PCE increases with temperature up to 450 K, if the temperature increases, the value of J_{SC} will increase due to the band gap reduction of the material and consequently, more number of electron-hole pairs will be generated [18]. The temperature started to decrease after 450 K, it is evident that as temperature increases, the power generation from the PV cell decreases and as a result, the PCE decreases [25]. However, the FF was varied in a random way until the temperature 410 K, then it started also to decrease continuously with temperature. The fluctuation of the FF (defined as the ability to deliver available power to a load generated by the solar cell) before 410 K is due to variation of conductivity [25] .The optimum temperature value deduced from this study that gives a maximum PCE of 17.29% and FF of 86.26% is 440 K which prove the stability of $BaZrS_3$ compound [26] .

The main objective behind our study was to simulate and optimize the cell parameters in order to obtain an optimum efficiency by using the absorber $BaZrS_3$ in the first time in SCAPS-1D software. Device optimization according to our results is presented in Table 5, which summarize the optimum valued of each parameters and for each layer.

J-V characteristic after enhancing all parameters except temperature (keeping the default value of 300 K) is shown in Fig. 8 that indicated the following values: PCE of 15.81%, FF of 87.13%, J_{SC} of 16.5340 mA/cm^2 and V_{oc} of 1.0973 V. As well as the characteristic after enhancing all parameters including the optimum temperature (440 K), is illustrated in Fig. 9 which gives the following final parameters: PCE of 17.29 %, FF f 86.26 %, V_{oc} of1.2124 V and J_{SC} of 16.5363 mA/cm^2.

Table 5
Optimized parameters after enhancement

Optimized parameters	Thickness (nm)	Doping density (cm^{-3})	Defect density (cm^{-3})
$BaZrS_3$	850	1×10^{20}	10^{13}
Spiro-OMeTAD	60	9×10^{19}	-
TiO_2	10	8×10^{19}	-
FTO	80	1×10^{19}	-

4.5. The quantum efficiency versus wavelength

The quantum efficiency (QE) of the solar cell value indicates the amount of current that the cell will produce when irradiated by photons of a particular wavelength [27], it is an important parameter that reveals the quality of solar cell's active layer. As illustrated in Fig. 10, the cell structure that we studied in this work has excellent quantum efficiency.

A comparison between the two absorbers Organic–inorganic halide perovskite $MAPbI_3$ and $BaZrS_3$ was made for the same structure FTO/TiO_2/Absorber/Spiro-OMeTAD/Au. To prove that $BaZrS_3$ could replace hybrid perovskites while keeping a better quality-price ratio. As explicated in Table 6.

Table 6. Comparison between $MAPbI_3$ and $BaZrS_3$

Simulation results	$MAPbI_3$[2]	$BaZrS_3$ (This work)
V_{OC} (V)	1.120	1.097
J_{SC} (mA/cm^2)	24.98	16.53
FF (%)	81.86	87.13
PCE (%)	23.04	15.81

Conclusion

In this work, we have shed light on the chalcogenide $BaZrS_3$ as an absorber material for solar cells. The simulation performed in our study was made using SCAPS-1D software, based on a specific approach in which each device parameter was varied individually (keeping the other parameters constant) in order to see its impact on the device performance specially on the PCE and FF. From our results, we can conclude that the absorber (active layer) is the most important material in the cell because of its higher impact on the performance of this later. The optimized (thickness, doping concentration) are set to be: (80 nm; 1×10^{19} cm^{-3}), (10 nm; 8×10^{19} cm^{-3}), (850 nm; 1×10^{20} cm^{-3}) and (60 nm; 9×10^{19} cm^{-3}) for FTO, TiO_2, $BaZrS_3$ and Spiro-OMeTAD materials respectively. Concerning defect density in the absorber, the optimal

value is fixed at 10^{13} cm^{-3}. As well as the optimum values of interfaces defect densities are: 10^{15} cm^{-2} for HTL/$BaZrS_3$ and 10^{11} cm^{-2} for $BaZrS_3$/ETL. In addition, our simulation results prove that increasing temperature from 300 K to 440 K enhance the PCE from 15.81% to 17.29% which it is not the case for Sn based PSC where the PCE decrease linearly with increase in temperature from 300 K to 400 K [25]. The final results, when including all parameters optimization are fixed at: PCE of 17.29%, FF of 86.26%, *Voc* of 1.2124 V and *Jsc* of 16.5363 mA/cm^2, with an excellent quantum efficiency. This simulation study will lead to understanding the operation mechanism, reduce the cost and increase the efficiency by using an optimized parameters which will helps in the improvement of the performance of chalcogenide perovskite solar cells.

References

[1] A. Kojima, K. Teshima, Y. Shirai, et T. Miyasaka, « Organometal Halide Perovskites as Visible-Light Sensitizers for Photovoltaic Cells », *J. Am. Chem. Soc.*, vol. 131, n° 17, p. 6050-6051, mai 2009, doi: 10.1021/ja809598r.

[2] Y. Raoui, H. Ez-Zahraouy, N. Tahiri, O. El Bounagui, S. Ahmad, et S. Kazim, « Performance analysis of MAPbI3 based perovskite solar cells employing diverse charge selective contacts: Simulation study », *Sol. Energy*, vol. 193, p. 948-955, nov. 2019, doi: 10.1016/j.solener.2019.10.009.

[3] H. Shaili, « Synthesis of the Sn-based CaSnS3 chalcogenide perovskite thin film as a highly stable photoabsorber for optoelectronic applications », *J. Alloys Compd.*, p. 9, 2021.

[4] K. Kuhar *et al.*, « Sulfide perovskites for solar energy conversion applications: computational screening and synthesis of the selected compound $LaYS_3$ », *Energy Environ. Sci.*, vol. 10, n° 12, p. 2579-2593, 2017, doi: 10.1039/C7EE02702H.

[5] M. Buffiere, D. S. Dhawale, et F. El-Mellouhi, « Chalcogenide Materials and Derivatives for Photovoltaic Applications », *Energy Technol.*, vol. 7, n° 11, p. 1900819, nov. 2019, doi: 10.1002/ente.201900819.

[6] A. Swarnkar, W. J. Mir, R. Chakraborty, M. Jagadeeswararao, T. Sheikh, et A. Nag, « Are Chalcogenide Perovskites an Emerging Class of Semiconductors for Optoelectronic Properties and Solar Cell? », *Chem. Mater.*, vol. 31, n° 3, p. 565-575, févr. 2019, doi: 10.1021/acs.chemmater.8b04178.

[7] X. Wei *et al.*, « Ti-Alloying of $BaZrS_3$ Chalcogenide Perovskite for Photovoltaics », *ACS Omega*, vol. 5, n° 30, p. 18579-18583, août 2020, doi: 10.1021/acsomega.0c00740.

[8] H. Zitouni, N. Tahiri, O. El Bounagui, et H. Ez-Zahraouy, « Electronic, optical and transport properties of perovskite BaZrS3 compound doped with Se for photovoltaic applications », *Chem. Phys.*, vol. 538, p. 110923, oct. 2020, doi: 10.1016/j.chemphys.2020.110923.

[9] M. G. Helander, M. T. Greiner, Z. B. Wang, W. M. Tang, et Z. H. Lu, « Work function of fluorine doped tin oxide », *J. Vac. Sci. Technol. Vac. Surf. Films*, vol. 29, n^{o} 1, p. 011019, janv. 2011, doi: 10.1116/1.3525641.

[10] M. Rouchdi, E. Salmani, B. Fares, N. Hassanain, et A. Mzerd, « Synthesis and characteristics of Mg doped ZnO thin films: Experimental and ab-initio study », *Results Phys.*, vol. 7, p. 620-627, 2017, doi: 10.1016/j.rinp.2017.01.023.

[11] M. M. Tavakoli, P. Yadav, R. Tavakoli, et J. Kong, « Surface Engineering of TiO_2 ETL for Highly Efficient and Hysteresis-Less Planar Perovskite Solar Cell (21.4%) with Enhanced Open-Circuit Voltage and Stability », *Adv. Energy Mater.*, vol. 8, n^{o} 23, p. 1800794, août 2018, doi: 10.1002/aenm.201800794.

[12] B. Parida, A. Singh, M. Oh, M. Jeon, J.-W. Kang, et H. Kim, « Effect of compact TiO2 layer on structural, optical, and performance characteristics of mesoporous perovskite solar cells », *Mater. Today Commun.*, vol. 18, p. 176-183, mars 2019, doi: 10.1016/j.mtcomm.2018.12.007.

[13] S. Fantacci, F. De Angelis, M. K. Nazeeruddin, et M. Grätzel, « Electronic and Optical Properties of the Spiro-MeOTAD Hole Conductor in Its Neutral and Oxidized Forms: A DFT/TDDFT Investigation », *J. Phys. Chem. C*, vol. 115, n^{o} 46, p. 23126-23133, nov. 2011, doi: 10.1021/jp207968b.

[14] M. Kumar, A. Singh, D. Gill, et S. Bhattacharya, « Optoelectronic Properties of Chalcogenide Perovskites by Many-Body Perturbation Theory », *J. Phys. Chem. Lett.*, vol. 12, n^{o} 22, p. 5301-5307, juin 2021, doi: 10.1021/acs.jpclett.1c01034.

[15] Y. Raoui, H. Ez-Zahraouy, S. Kazim, et S. Ahmad, « Energy Level Engineering of Charge Selective Contact and Halide Perovskite by Modulating Band Offset: Mechanistic Insights », preprint, mai 2020. doi: 10.26434/chemrxiv.12367505.v1.

[16] None Available, « Materials Data on BaZrS3 by Materials Project ». LBNL Materials Project; Lawrence Berkeley National Laboratory (LBNL), Berkeley, CA (United States), 2020. doi: 10.17188/1264764.

[17] Y. Ahmed, « Fill Factor and Efficiency », *24 Solar Home*, oct. 31, 2013. http://24solarhome.com/fill-factor-and-efficiency/ (consulté le oct. 17, 2021).

[18] K. Chakraborty, M. G. Choudhury, et S. Paul, « Numerical study of Cs2TiX6 (X = Br−, I−, F− and Cl−) based perovskite solar cell using SCAPS-1D device simulation », *Sol. Energy*, vol. 194, p. 886-892, déc. 2019, doi: 10.1016/j.solener.2019.11.005.

[19] R. N. Chauhan, C. Singh, R. S. Anand, et J. Kumar, « Effect of Sheet Resistance and Morphology of ITO Thin Films on Polymer Solar Cell Characteristics », *Int. J. Photoenergy*, vol. 2012, p. 1-6, 2012, doi: 10.1155/2012/879261.

[20] K. Tan, P. Lin, G. Wang, Y. Liu, Z. Xu, et Y. Lin, « Controllable design of solid-state perovskite solar cells by SCAPS device simulation », *Solid-State Electron.*, vol. 126, p. 75-80, déc. 2016, doi: 10.1016/j.sse.2016.09.012.

[21] Md. S. Rahman, S. Miah, M. S. W. Marma, et T. Sabrina, « Simulation based Investigation of Inverted Planar Perovskite Solar Cell with All Metal Oxide Inorganic Transport Layers », in *2019 International Conference on Electrical, Computer and Communication Engineering (ECCE)*, Cox'sBazar, Bangladesh, févr. 2019, p. 1-6. doi: 10.1109/ECACE.2019.8679283.

[22] B. M. Soucase, I. Guaita Pradas, et K. R. Adhikari, « Numerical Simulations on Perovskite Photovoltaic Devices », in *Perovskite Materials - Synthesis, Characterisation, Properties, and Applications*, L. Pan et G. Zhu, Éd. InTech, 2016. doi: 10.5772/61751.

[23] U. Mandadapu, Department of Physics, Madanapalle Institute of Technology and Science, Madanapalle - 517325, Chittoor, Andhra Pradesh, India, S. V. Vedanayakam, Department of Physics, Madanapalle Institute of Technology and Science, Madanapalle - 517325, Chittoor, Andhra Pradesh, India, K. Thyagarajan, et Department of Physics, JNTU College of Engineering Pulivendula - 516390, Andhra Pradesh, India, « Simulation and Analysis of Lead based Perovskite Solar Cell using SCAPS-1D », *Indian J. Sci. Technol.*, vol. 10, n° 11, p. 1-8, mars 2017, doi: 10.17485/ijst/2017/v10i11/110721.

[24] S. Abdelaziz, A. Zekry, A. Shaker, et M. Abouelatta, « Investigating the performance of formamidinium tin-based perovskite solar cell by SCAPS device simulation », *Opt. Mater.*, vol. 101, p. 109738, mars 2020, doi: 10.1016/j.optmat.2020.109738.

[25] P. Roy, N. Kumar Sinha, et A. Khare, « An investigation on the impact of temperature variation over the performance of tin-based perovskite solar cell: A numerical simulation approach », *Mater. Today Proc.*, vol. 39, p. 2022-2026, 2021, doi: 10.1016/j.matpr.2020.09.281.

[26] C. Comparotto *et al.*, « Chalcogenide Perovskite $BaZrS_3$: Thin Film Growth by Sputtering and Rapid Thermal Processing », *ACS Appl. Energy Mater.*, vol. 3, n° 3, p. 2762-2770, mars 2020, doi: 10.1021/acsaem.9b02428.

[27] « Quantum efficiency », *Wikipedia*. nov. 01, 2021. Consulté le: janv. 11, 2022. [En ligne]. Disponible sur: https://en.wikipedia.org/w/index.php?title=Quantum_efficiency&oldid=1053106456

Figures

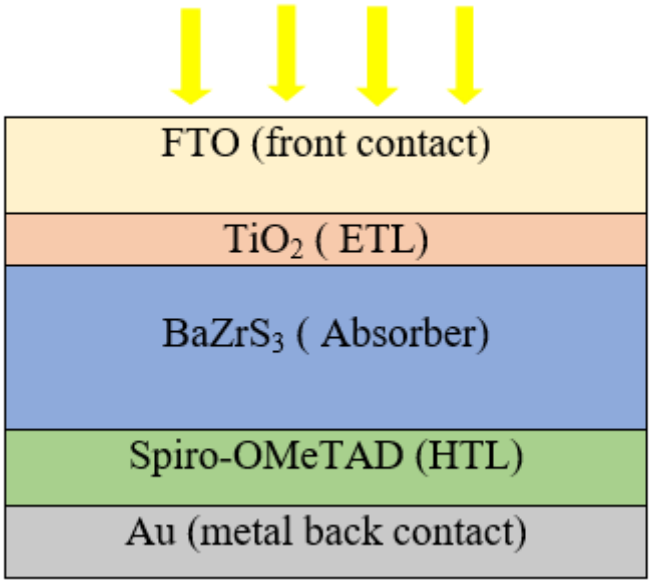

Figure 1

Solar cell structure

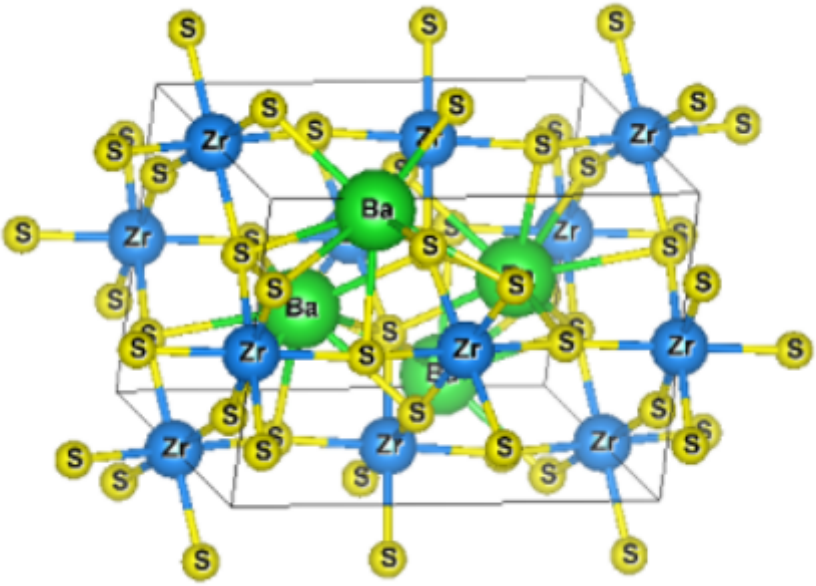

Figure 2

The structure of $BaZrS_3$ by Vesta software

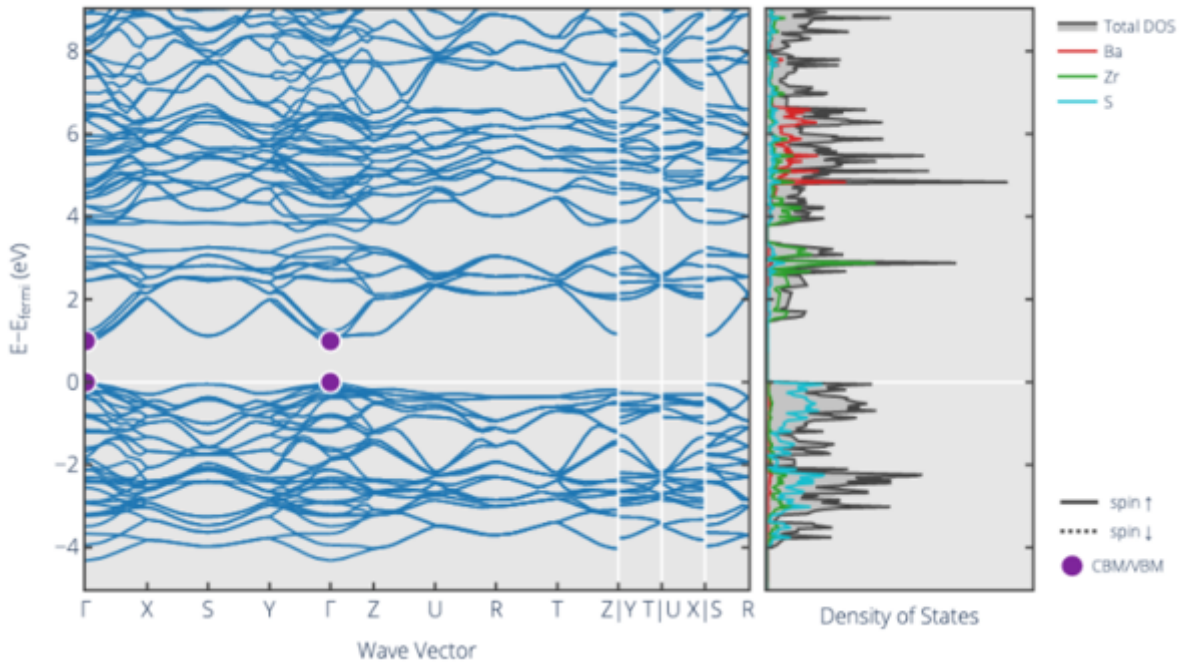

Figure 3

Band structure and Density of states correspond to $BaZrS_3$[16]

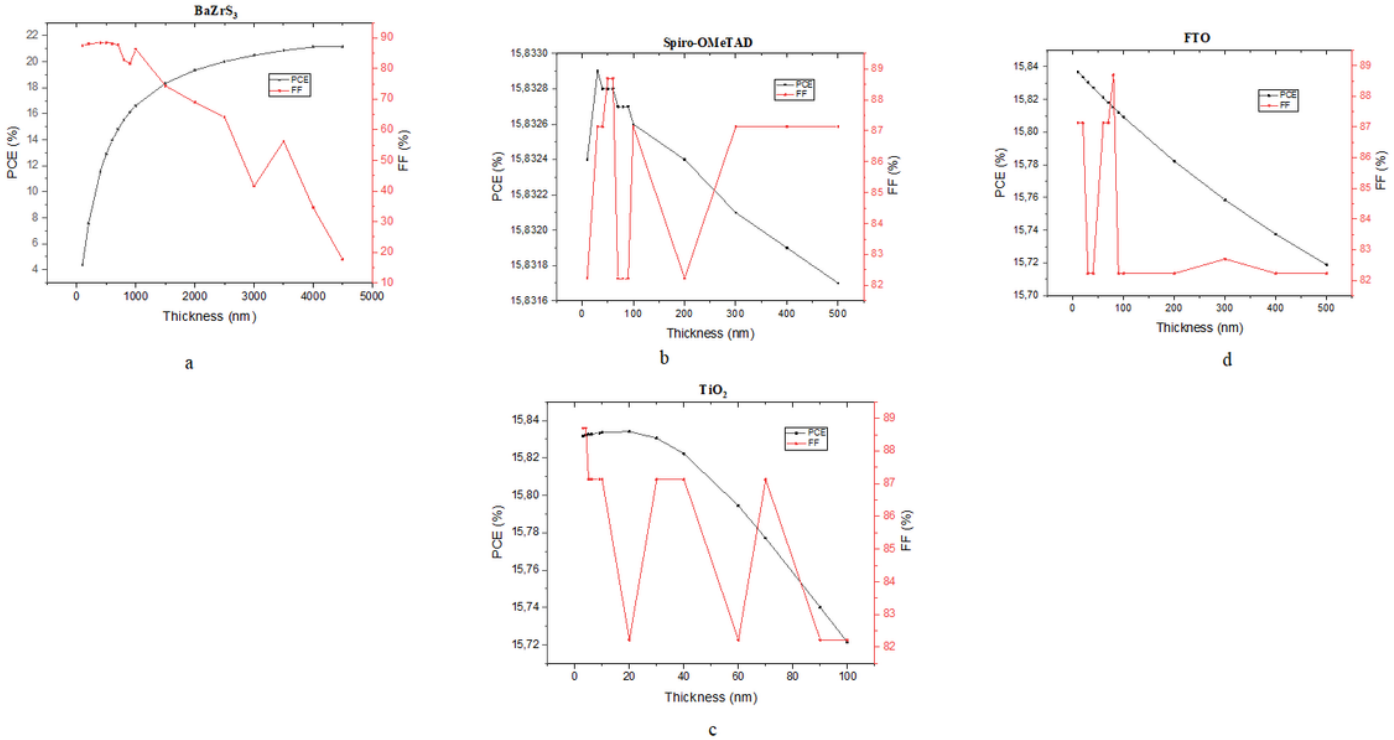

Figure 4

(a) PCE and FF as a function of the absorber thickness

(b) PCE and FF as a function of the HTM thickness

(c) PCE and FF as a function of the ETM thickness

(d) PCE and FF as a function of FTO thickness

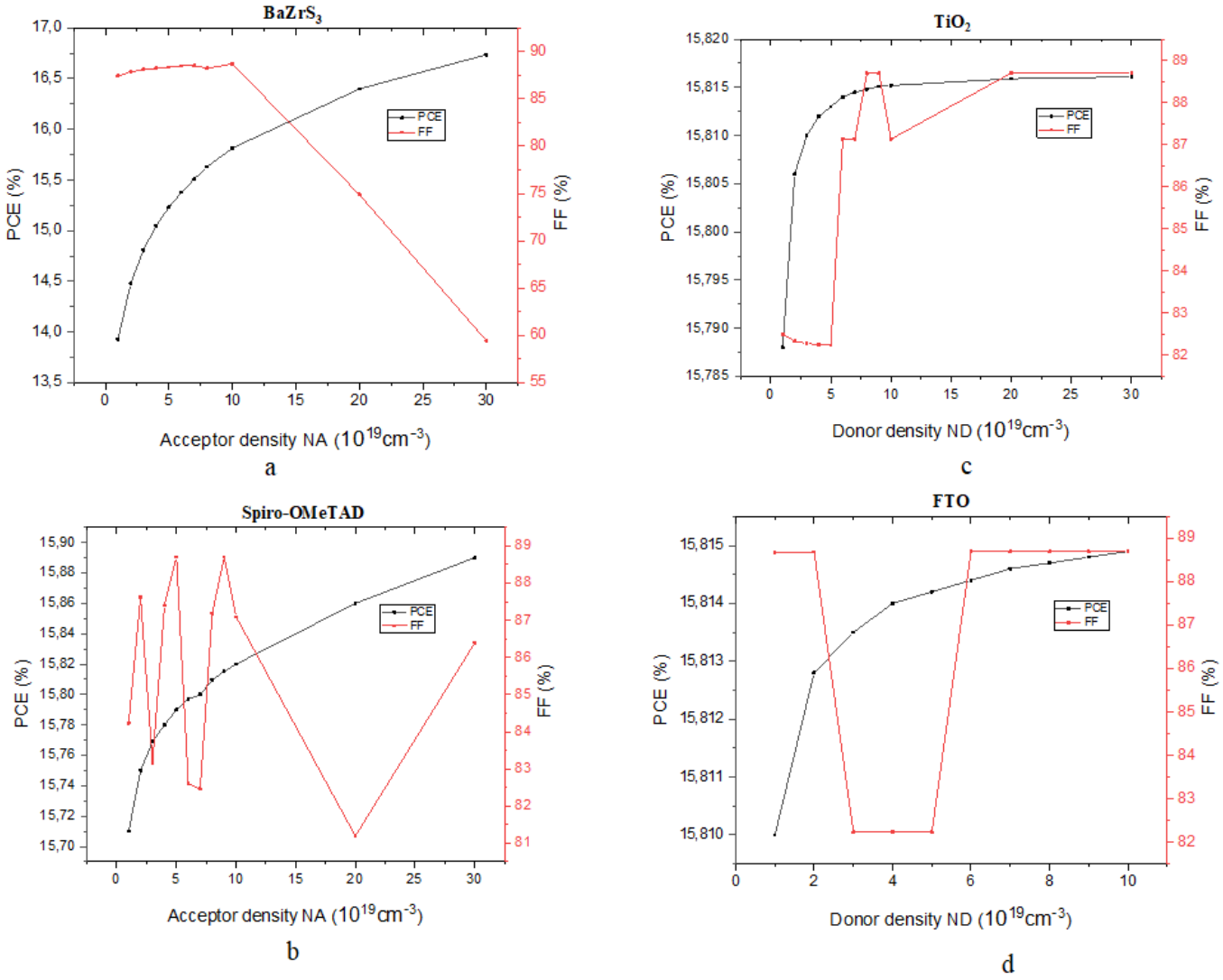

Figure 5

(a) PCE and FF as a function of the absorber Acceptor density

(b) PCE and FF as a function of the HTL Acceptor density

(c) PCE and FF as a function of the ETL Donor density

(d) PCE and FF as a function of the FTO Donor density

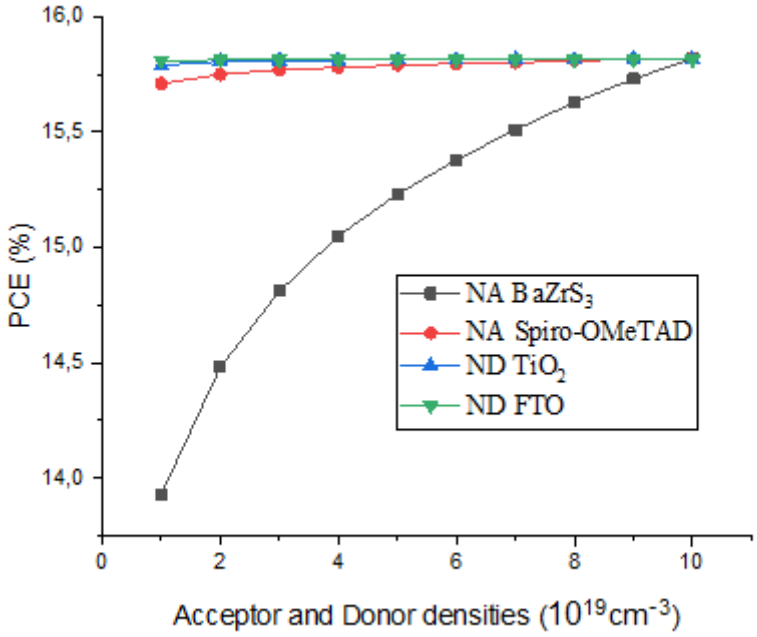

Figure 6

Comparison of doping densities effect for each layer

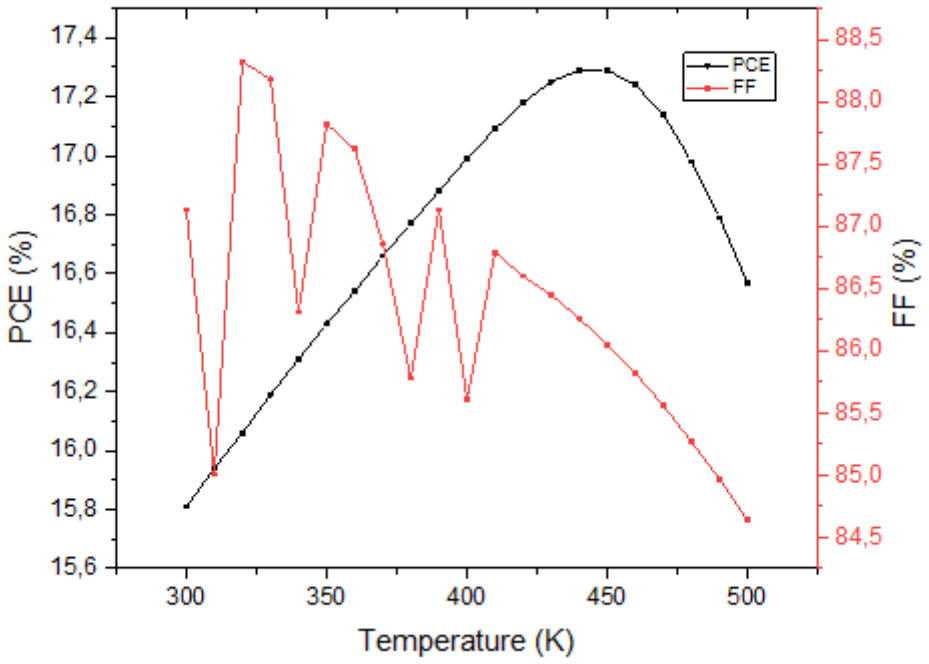

Figure 7

Impact of temperature on the PCE and FF

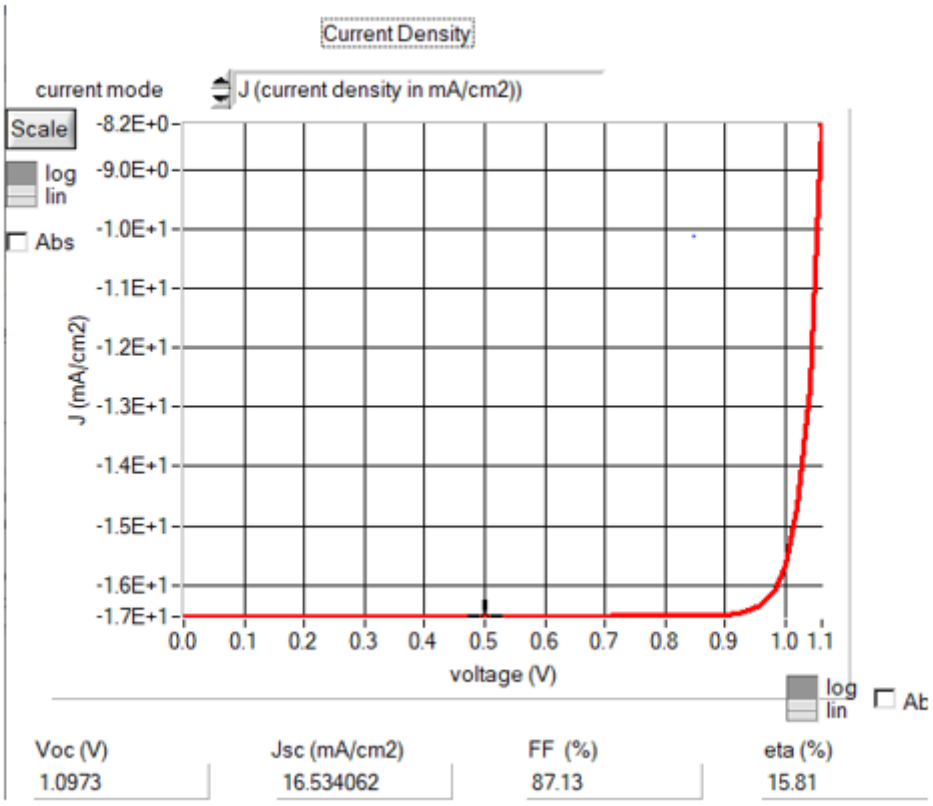

Figure 8

J-V curve after enhancement at 300 K

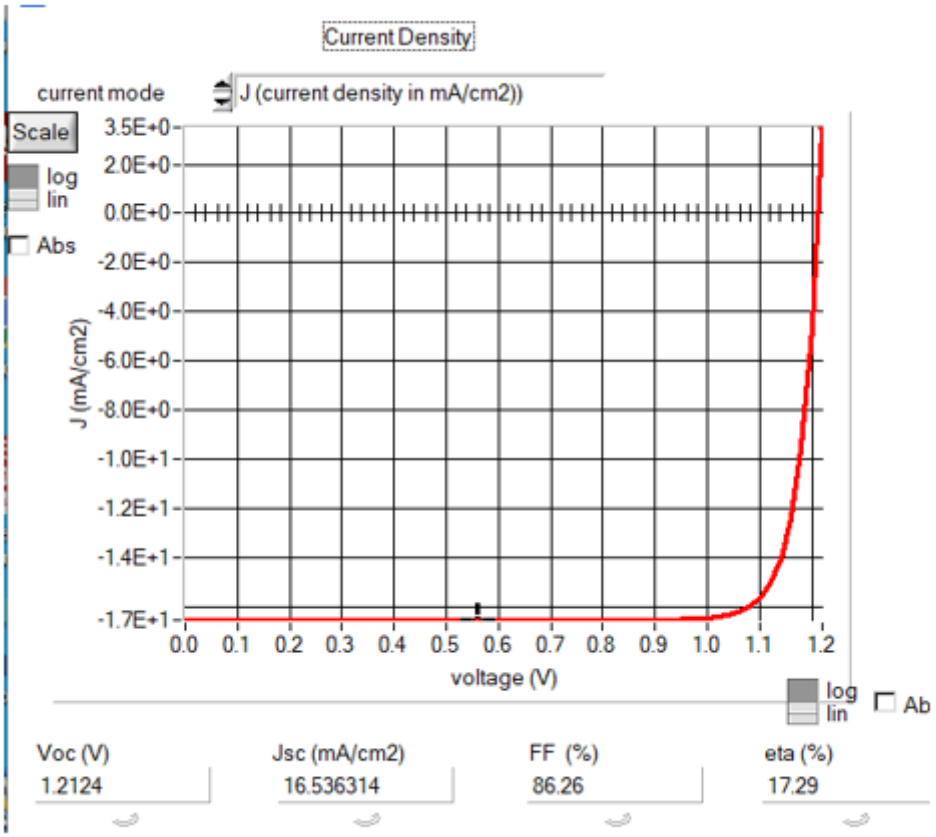

Figure 9

J-V curve after enhancement with an optimized temperature of 440 K

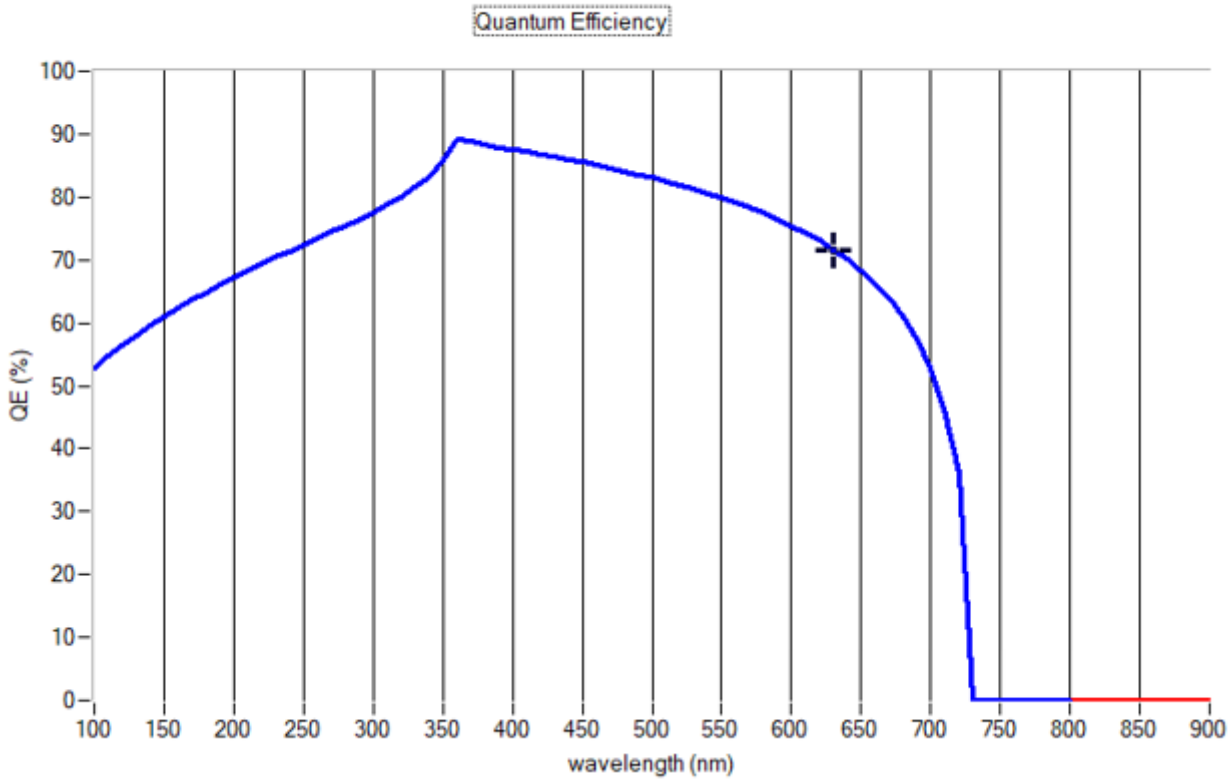

Figure 10

Simulated QE curve with all optimized parameters except temperature